# scientific reports

OPEN

# Plasma loaded uniaxial chiral slab waveguide

Muhammad Umair[1], Abdul Ghaffar[1]✉, Majeed A. S. Alkanhal[2], Yasin Khan[2], Muhammad Usman Shahid[1] & Muhammad Amir Ali[3]

In this study, numerical analysis has been carried out at plasma loaded uniaxial chiral slab waveguide. The formulation is based on differential form of Maxwell's equations and characteristics equation is obtained by employing boundary conditions at uniaxial chiral-plasma-uniaxial. Two cases of uniaxial chiral media i.e., axial permitivity grater than tranverse permitivity and axial permitivity less than tranverse permitivity are discussed to explore the characteristics for proposed waveguide structure. The influence of collsional frequencies, plasma frequencies, chirality and core width of waveguide on normalized propagation constant and propagation are analyzed. Numerical results indicate that physical parametrs of isotropic plasma (collisonal frequency and plasma frequency), chirality and core width play pivotal role to tune the normlized propagation constant, propagation length band gap and cut-off frequency in certain frequency range. The extraordinary traits of uniaxial chiral and plasma medium offer a wide range of research and development possibilities in diverse areas of optoelectronics.

Electromagnetic surface wave propagation are of recent interest due to their modern applications in spectroscopy[1–4], optical sensing, chemical sensing and communication system[5]. Electromagnetic surface wave propagate between two dissimilar media and shows attenuation. Different types of electromagnetic surface waves excited by using different optical materials. i.e., Surface plasmon polaritons excited at the metal dielectric interface. The term "Fano wave" is commonly used to describe a specific type of surface plasmon polariton (SPP) wave[6]. This term is employed when the imaginary part of the permittivity of a metal is significantly smaller as compared to the real part of the permittivity. Dyakonov wave supported at two dielectric materials one of them should be anisotropic[7–9]. The properties of electromagnetic surface wave depneds upon partening optical materials. In optics community, the analysis of plasma filled parallel plate waveguide structures (PPWG) exhibit remarkable features to fabricate microwave devices[10–14]. The interaction between electromagnetic waves and isotropic plasma can be characterized by absorption, reflection, or transmission, depending on the wavelength and size of the plasma medium[15,16] and has pottential application in high frequency applications[17]. The determination of absorption, reflection, and transmission characteristics in a plasma medium involves analyzing the plasma frequency, collisional frequency, and electromagnetic wave frequency. The permitivity of isotropic plasma medium i.e., (real and imaginary) are acquired by plasma features (plasma frequency and collsional frequency) and electromagnetic waves frequency. By manipulating the complex permittivity and number density of electrons, one can affect the effective collisional frequency and plasma oscillation frequency, which in turn determine the behavior of the electromagnetic field in isotropic plasma medium[15]. Various nonlinear complex differential equations have been analyzed for plasmonics community[18,19]. In this context, researchers have extensively explore the properties of electromagnetic surface waves. For example, Xu et al. explored the characteristics of s-ploarized and p-plarized surface waves in indefinite medium waveguide[20]. Y. Cao et al. studied nonliner absoroption of plasma filled cyliderical waveguide[21]. L. Zheng et al. analyzed the reflection and transmission of electromagnetic wave in isotropic plasma filled structure at THz frequency regime[22]. G. Xu & Z. Song the studied the reflection and transmission characteristics of plasma filled medium in slab waveguide structure[23]. C. X. Yuan et al. explored the characteristics of plasma filled slab waveguide by using FDTD method[24]. Smirnov and Valovik examined the propagation of transverse electric (TE) guided waves in Kerr-type nonlinear filled PPWG. They found that when nonlinearity was introduced, a great deal of interesting results was observed for propagation modes that did not present in linear wave[25]. Rashid et al. analyzed the TE waves in plasma filled PPWG sorrouded by ferrite films to design and implementation of integrated circuit and antenna system at mirowave frequencies[26]. M.N. Shaikh demonstrated the numerical analysis of plasma

[1]Department of Physics, University of Agriculture, Faisalabad, Pakistan. [2]Department of Electrical Engineering, King Saud University, Riyadh, Saudi Arabia. [3]School of Materials Science and Engineering, Zhengzhou University, Zhengzhou 450001, China. ✉email: aghaffar16@uaf.edu.pk

sandwich between left handed material (LHM) to fabricate the split ring resonator of LHM. They derived the dispersion relation for transverse electric mode. Furthermore, they analyzed the propagation constant versus wave frequency for different plasma thicknesses, plasma frequency and physical parametrs of LHM[27]. B. Zamir and R. Ali explored the transverse electric characteristics of plamsa medium sorrounded by nonolinear magnetic materials. They studied the propagation constant and power flow for physical parametr of isotropic plasma medium as well as nonlinera metamaterials at microwave frequencies to fabricate nanophotonic devices.

Recnetaly, metamaterial attracted much attention in optics sector[28,29]. The uniaxial chiral mediums are special type of chiral mediums in which chirality does not appear to be directional[30]. The process of artificially producing uniaxial chiral media is quite simple[31]. Small chiral items (such as wire spirals) are usually immersed into anisotropic host media to synthesize uniaxial chiral materials[32]. It is widely recognized that to manufacture isotropic chiral material, an arbitrary arrangement of spirals is essential, which is complicated and expensive[33]. One of other disadvantages of isotropic chiral material is that once it has been manufactured, it is relatively difficult to control its degree of chirality. A waveguide including uniaxial chiral medium is expected to possess some extraordinary features due to the presence of chirality combined with anisotropy. Furthermore, it enables complete control over chirality[34]. That is also the reason for our interest in studying plasma loaded uniaxial chiral slab waveguide.

The above mentioned literature authors mainly focus on exploring the influence of homogeneous plasma and an inhomogeneous plasma on EM surface wave and have achieved abundant meaningful results. However, the EM surface waves in plasma loaded uniaxial chiral slab is not presented yet. In this manuscript, plasma loaded uniaxial chiral slab waveguide is analyzed to explore hybrid surface wave properties. Two cases of uniaxial chiral media i.e., $\epsilon_z > \epsilon_t$ and $\epsilon_t > \epsilon_z$ are analyzed. Frequency dependent normalized propagation cosntant and propagation length under different values of plasma features (plasma frequency and collsional frequency), core width and chirality are studied.

## Methodology

Three layers geometry for plasma loaded uniaxial chiral slab waveguide is shown in Fig. 1. Medium I and medium III represent uniaxial chiral medium while medium II isotropic plasma. Electromagnetic waves propagate along z-axis and attenuate along x-axis.

The constitutive relations for uniaxial chiral medium are given below.

$$\begin{aligned} \boldsymbol{D} &= \left[ \varepsilon_t \overline{\overline{I}}_t + \varepsilon_z \hat{e}_z \hat{e}_z \right] . \mathrm{E} - j\xi\sqrt{\mu_0\varepsilon_0}\hat{e}_z\hat{e}_z . \mathrm{H} \\ \boldsymbol{B} &= \left[ \mu_t \overline{\overline{I}}_t + \mu_z \hat{e}_z \hat{e}_z \right] . \mathrm{H} - j\xi\sqrt{\mu_0\varepsilon_0}\hat{e}_z\hat{e}_z . \mathrm{E} \end{aligned} \tag{1}$$

In Eq. 1, $\xi$ represent the chirality parameter which is responsible for electromagnetic coupling, $\overline{\overline{I}}_t = \hat{e}_x\hat{e}_x + \hat{e}_z\hat{e}_z$ is a dyadic vector, $\epsilon_0$ and $\mu_0$ are the permittivity and permeability of free space, respectively, $\epsilon_t, \mu_t$, and $\epsilon_z$, $\mu_z$ are transverse and longitudinal components of uniaxial chiral medium, and $\widehat{e}_x, \widehat{e}_y$, and $\widehat{e}_z$ are mutually perpendicular unit vectors in a Cartesian coordinate system. The time dependency $e^{j\omega t}$ is taken.

### EM field components for medium I

$$\mathrm{E}_z = C_1\, e^{-k_1 x} + C_2\, e^{-k_2 x} \tag{2}$$
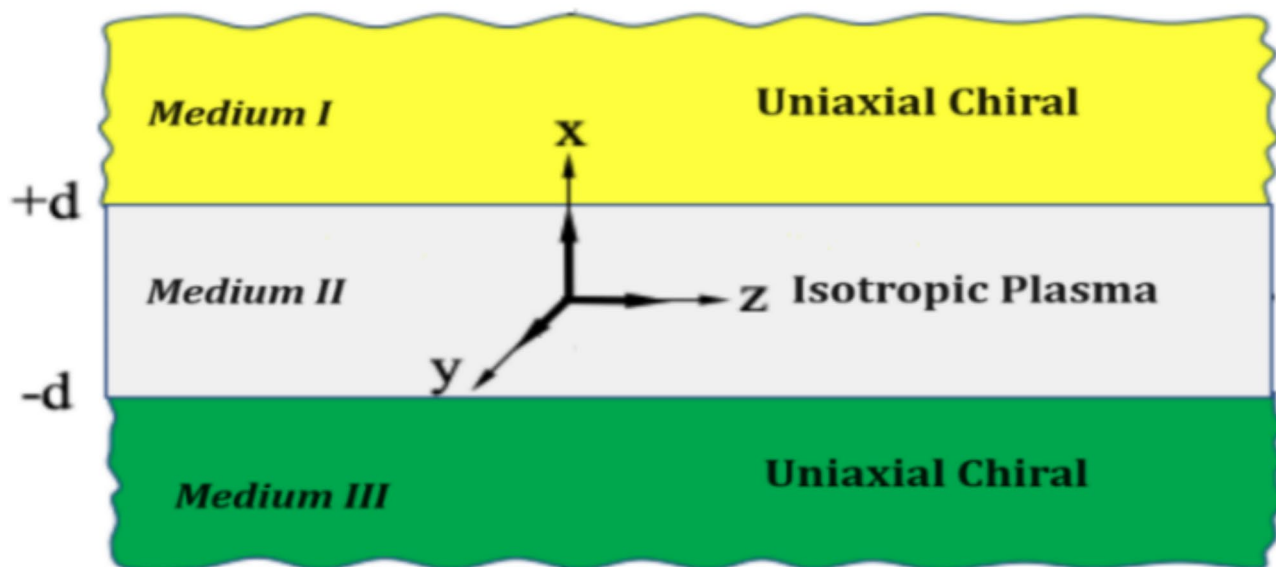


**Fig. 1**. Geometry for plasma loaded uniaxial chiral slab waveguide.

$$H_z = \frac{j\alpha_{1,2}}{\eta_t}\left(C_1\,e^{-k_1 x} + C_2\,e^{-k_2 x}\right) \tag{3}$$

Here, $k_1$ and $k_2$ are wavenumbers for uniaxial chiral medium. The remaining EM fields components can be obtained from[35].

$$k_1{}^2 = \frac{\lambda^2}{2}\left[\frac{\mu_z}{\mu_t} + \frac{\epsilon_z}{\epsilon_t} + \sqrt{\left(\frac{\mu_z}{\mu_t} - \frac{\epsilon_z}{\epsilon_t}\right)^2 + \frac{4\varpi\,\xi^2 \mu_z \epsilon_z}{\mu_t \epsilon_t}}\right] \tag{4}$$

$$k_2{}^2 = \frac{\lambda^2}{2}\left[\frac{\mu_z}{\mu_t} + \frac{\epsilon_z}{\epsilon_t} - \sqrt{\left(\frac{\mu_z}{\mu_t} - \frac{\epsilon_z}{\epsilon_t}\right)^2 + \frac{4\xi^2 \mu_z \epsilon_z}{\mu_t \epsilon_t}}\right] \tag{5}$$

$$\lambda^2 = \beta^2 - \omega^2 \mu_t \epsilon_t \tag{6}$$

$$\alpha_1 = \left(\frac{q_1{}^2}{\lambda^2} - \frac{\epsilon_z}{\epsilon_t}\right)\frac{\sqrt{\mu_t \epsilon_t}}{\xi\,\sqrt{\mu_z \epsilon_z}} \tag{7}$$

$$\alpha_2 = \left(\frac{q_2{}^2}{\lambda^2} - \frac{\epsilon_z}{\epsilon_t}\right)\frac{\sqrt{\mu_t \epsilon_t}}{\xi\,\sqrt{\mu_z \epsilon_z}} \tag{8}$$

$$\eta = \sqrt{\epsilon_t/\mu_t} \tag{9}$$

### EM field components for medium II

$$H_z = C_5\,e^{k_p x} + C_6\,e^{-k_p x} \tag{10}$$

$$E_z = C_7\,e^{k_p x} + C_8\,e^{-k_p x} \tag{11}$$

$$E_y = \frac{1}{j\omega\,\epsilon_p}\frac{d}{dx}(H_z) \tag{12}$$

$$H_y = -\frac{1}{j\omega\,\mu_0}\frac{d}{dx}(E_z) \tag{13}$$

Here, $C_1$, $C_2$, $C_3$, and $C_4$ are amplitude constants, and $k_p = \sqrt{\beta^2 - \omega^2\epsilon_p\mu_0}$, $k_0 = \omega\sqrt{\mu_0\epsilon_0}$, $\epsilon_p$ is the permittivity of isotropic plasma medium, $\epsilon_p = 1 - \frac{\omega_p{}^2}{\omega^2 + j\nu\,\omega}$, $\omega_p$ and $\nu$ are plasma frequency and collisional frequency respectively as reported in[15].

### EM field components for medium III

$$E_z = C_3\,e^{k_1 x} + C_4\,e^{k_2 x} \tag{14}$$

$$H_z = \frac{j\alpha_{1,2}}{\eta_t}\left(C_3\,e^{k_1 x} + C_4\,e^{k_2 x}\right) \tag{15}$$

The remaining EM fields components can be obtained from[35]. By using the above EM field equation for uniaxial chiral and plasma medium the following boundary conditions are employed to obtain the characteristics equation:

$$\widehat{x}\times[H_1 - H_2] = 0 \tag{16}$$

$$\widehat{x}\times[E_1 - E_2] = 0 \tag{17}$$

The above boundary conditions to be enforced at uniaxial chiral-plasma-uniaxial chiral to obtain following characteristics Eq.

$$\begin{aligned}
&(-(\alpha_1 - \alpha_2)\eta\,(k_1 k_2 k_p^2 + k_t^2 \alpha_1\alpha_2\varepsilon_p\mu_0\omega^2 + (k_1 k_2 k_p^2 - k_t^2\alpha_1\alpha_2\varepsilon_p\mu_0\omega^2)\cosh[2dk_p])\\
&- k_t(k_2\alpha_1 - k_1\alpha_2)k_p(-\varepsilon_p\eta^2 + \alpha_1\alpha_2\mu_0)\omega\,\sinh[2dk_p]) = 0
\end{aligned} \tag{18}$$

## Results and discussion

In this section, electromagnetic surface wave features at uniaxial chiral-plasma-uniaxial chiral planar structure are analyzed at MHz frequency. For the surface wave analysis, the plots of characteristics curve under the different magnitudes of collisional frequencies, plasma frequencies, chirality and core width are discussed for three cases of uniaxial chiral media. The influence of isotropic plasma features, core width and chirality on normalized propagation constant and propagation length are analyzed. Low frequency and high frequency modes are

discussed. The numerical analysis of this work has been carried out at parameters i.e., $d = 60 \times 10^{-6}\, m$, $\mu_t = \mu_z = \mu_0$, $\mu_0 = 4\pi \times 10^{-7}$, $\omega_p = 4 \times 10^{10}\, Hz$ and $\nu = 20 \times 10^{10}\, Hz$. We assumed over dense plasma regime that plays a significant role in several theoretical and experimental research[26,27,36,37]. Introducing over dense plasma into waveguide systems can significantly enhance their performance. The high electron density alters the dispersion properties, leading to reduced losses and improved mode confinement. This effect enables the transmission of high-power and high-frequency signals with reduced energy dissipation.

### Case I $\epsilon_t > \epsilon_z$

To investigate this case, we have chosen parameters values for uniaxial chiral medium as: $\mu_t = \mu_z = \mu_0$, $\epsilon_t = -0.26\epsilon_0$ and $\epsilon_z = 0.4\epsilon_0$. Figure 2a analyzes the influence of collisional frequency on normalized propagation constant. The collisional frequency magnitudes increase from $\nu = 20 \times 10^{10}\, Hz$ to $\nu = 24 \times 10^{10}\, Hz$. In this context, two types of surface wave modes appear due to the anisotropic nature of chiral medium. It is observed that frequency band becomes narrow as the collision frequency of the plasma increases for both higher and lower modes. Furthermore, as collisional frequency increases, cut-off frequency starts increasing for both modes. The cut-off frequency is a vital parameter in electronic circuits as it determines the frequency range over which a filter operates effectively. By carefully selecting the cut-off frequency, engineers can design circuits that filter out unwanted frequencies and ensure the desired signals are transmitted or received accurately. The normalized propagation constant increases with frequency for each mode. At lower frequencies, the normalized propagation constant is smaller, meaning weaker confinement or slower wave propagation, while at higher frequencies, the propagation constant increases. The tunability of collisional frequency plays a crucial role in fine-tuning electromagnetic surface waves for communication systems. The variation in propagation length for three different values of collisional frequencies are revealed in Fig. 2b. Moreover, higher mode shows higher variation in band gap as compared to lower mode. The propagation length decreases with increasing frequency, which means higher frequencies correspond to shorter propagation distances due to increased losses or confinement in the medium. Figure 3a shows the plasma frequency dependence of characteristics curves on the normalized propagation constant as the function of operating frequency. The plasma frequency is directly proportional to the square root of the electron number density present in plasma medium, meaning that a higher electron density will result in a higher plasma frequency. As plasma frequency grows red shift occurs and normalized propagation constant enlarge for both modes as reported in[38]. Furthermore, at lower plasma frequencies ($\omega_p$), waves propagate with lower normalized constants. As plasma frequency increases ($\omega_p$), the waves can propagate faster, potentially implying tighter confinement of energy or better wave-guiding efficiency. Figure 3b analyzes the impact of plasma frequency on propagation length. As plasma frequency magnitude increases, band gap starts squeezing and characteristics curves move towards low frequency region for both modes. Additionally, lower mode shows unphysical at higher incident frequencies. It is concluded that physical parameters of isotropic plasma (collisional frequency and plasma frequency) are crucial features to tune the traits of electromagnetic surface waves in the fabrication of nanophotonic devices. Their careful manipulation enables the optimization of device performance, leading to advancements in various fields, including telecommunications, photonics, and quantum technologies. The dependance of core width on the normalized propagation constant is depicted in 4a. Core width increases from $d = 60 \times 10^{-6}\, m$ to $d = 70 \times 10^{-6}\, m$.
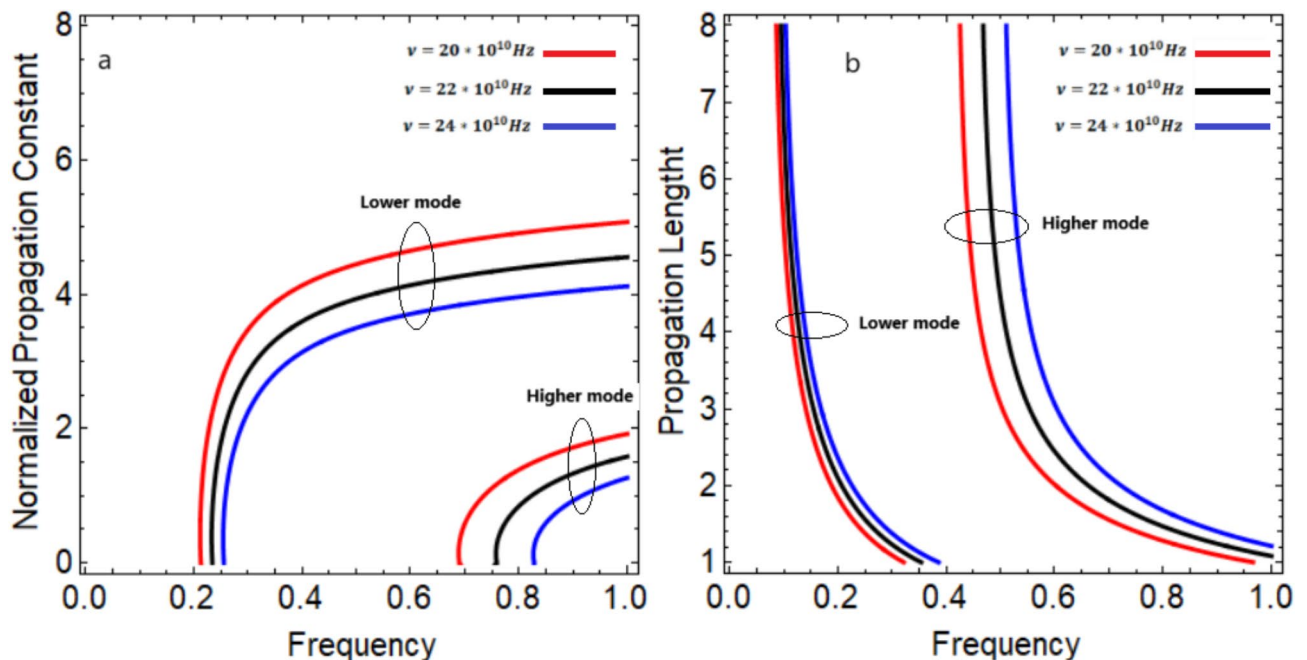


**Fig. 2.** Influence of collisional frequency on normalized propagation constant and propagation length.
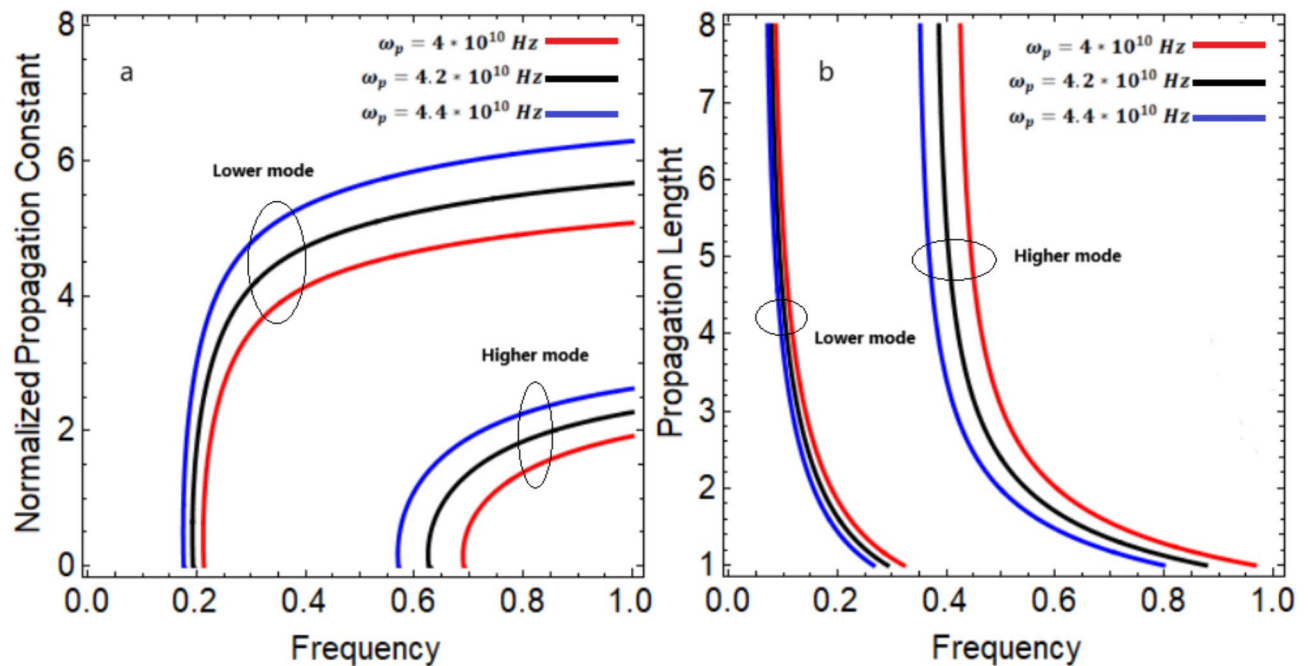
**Fig. 3**. Influence of plasma frequency on normalized propagation constant and propagation length.

As cut-off frequency decreases normalized propagation constant increases for both modes. It is also observed that as core width increases the band gap becomes narrow, and characteristics curves are shifted towards low frequency regions. Additionally, with the enhancement of core width, the normalized propagation constant also increases for both modes[38,39], leading to higher phase velocity and reduced modal dispersion. The influence of core width on propagation length is presented in Fig. 4b. Higher core width values decreases incident frequency and decreases band gap leading to the lower propagation length for both modes[38]. Furthermore, the variation in characteristic curve is smaller for smaller values of core width for both modes. To analyze the influence of chirality on the normalized propagation constant is depicted in Fig. 5a. As chirality increases, frequency band becomes broadened for both modes and cut-off frequency remains same for both modes. Furthermore, higher chirality values lead to higher normalized propagation constant for both modes[40,41]. Integrating chirality into photonic circuits provides new opportunities for on-chip light manipulation and signal processing. Frequency dependent propagation length under three different values of chirality is presented in Fig. 5b. One can observe that when chirality increases from $\xi = 1.1$ to $\xi = 1.18$ frequency band drastically reduces. Obviously, as chirality grows the band gap of both modes becomes narrow. Furthermore, increase in chirality, downshift the propagation length.

### Case II $\epsilon_t > \epsilon_z$

To analyze this case, we have selected parameters values for uniaxial chiral medium as: $\mu_t = \mu_z = \mu_0$, $\epsilon_t = 1.46\epsilon_0$ and $\epsilon_z = -1.1\epsilon_0$. The variations in propagation mode for normalized propagation constant and propagation length under the different values of collisional frequencies are investigated in Fig. 6a and b respectively. In Fig. 6a as magnitude of collisional frequency increases, the cut-off frequency of both modes increases while normalized propagation constant decreases for both modes. The cut-off frequency effect is a significant limitation that affects the performance and operational range of nanophotonic devices. By employing appropriate collisional frequency selection, the cut-off effect can be mitigated, allowing for the development of more versatile and efficient nanophotonic devices. The variation in propagation length for different collisional frequencies is depicted 6b. It is observed that propagation length is increased with increasing collisional frequency. Furthermore, higher collisional frequency shift characteristics curve higher incident wave frequency region. Additionally, frequency band starts squeezing for higher collisional frequencies for both modes. It is concluded that frequency band for both modes can be tuned by tuning the collisional frequency of plasma medium. By carefully selecting the appropriate frequency band, researchers and engineers can optimize the performance of nanophotonic devices, enabling advancements in the waveguide community. Figure 7a shows the variations of normalized propagation constant along with the EM wave frequency and plasma frequency. We can see that normalized propagation constant increases with decreasing EM wave frequency for both modes. Additionally, higher plasma frequency values lead to lower cut-off frequency for higher mode. Because when the plasma frequency is high, the charged particles are already oscillating at a significant rate. As a result, the external electromagnetic wave is unable to exert a strong influence on the charged particles, consequently cut-off frequency decreases.

Furthermore, in plasma physics research, understanding the relationship between plasma frequency and cut-off frequency is crucial for designing and studying plasma-based devices such as waveguides, resonators,
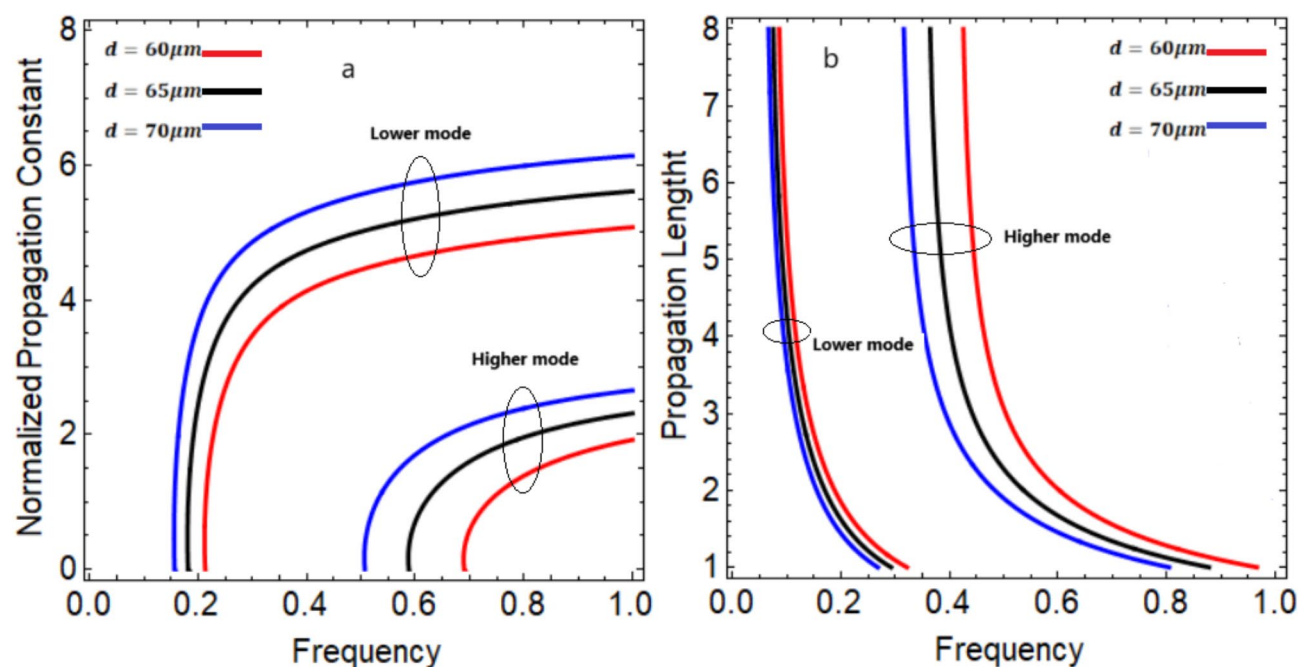
**Fig. 4**. Influence of core width on normalized propagation constant and propagation length.
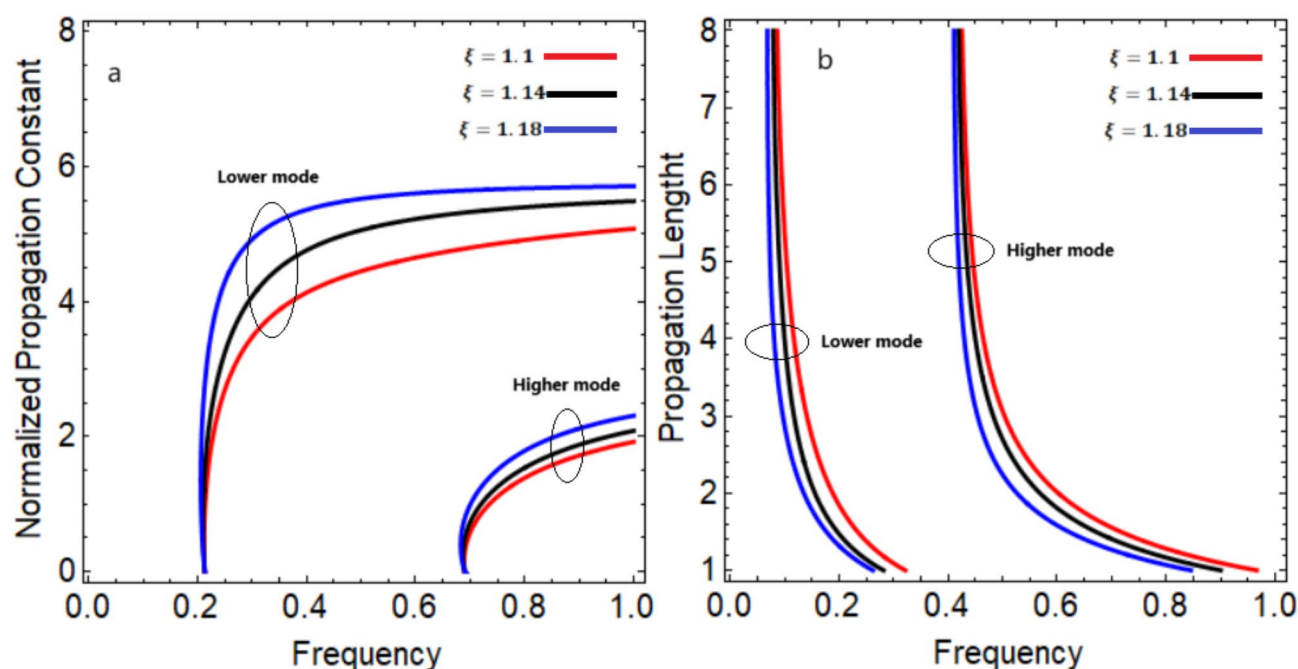


**Fig. 5**. Influence of chirality on normalized propagation constant and propagation length.

and filters. By controlling the plasma frequency, researchers can manipulate the cut-off frequency and tailor the performance nanophotonic devices according to their specific requirements. Figure 7b presents the influence of plasma frequency on propagation length. As seen from the presented characteristics curves, both modes are strongly influenced by plasma frequency. Numerical investigations showed that higher plasma frequencies will shift the characteristics curves of both modes in low frequency regions. Furthermore, lower mode exhibits smaller variation in frequency band gap as compared to higher mode. Figure 8a analyzes the effect of core width on normalized propagation constant. It is observed that for proposed waveguide structure; by increasing core width the cut-off frequency of both modes starts decreasing. By considering Fig. 8a it can be noted that as the core width increases, the normalized propagation constant also increases as reported in[42,43], allowing for
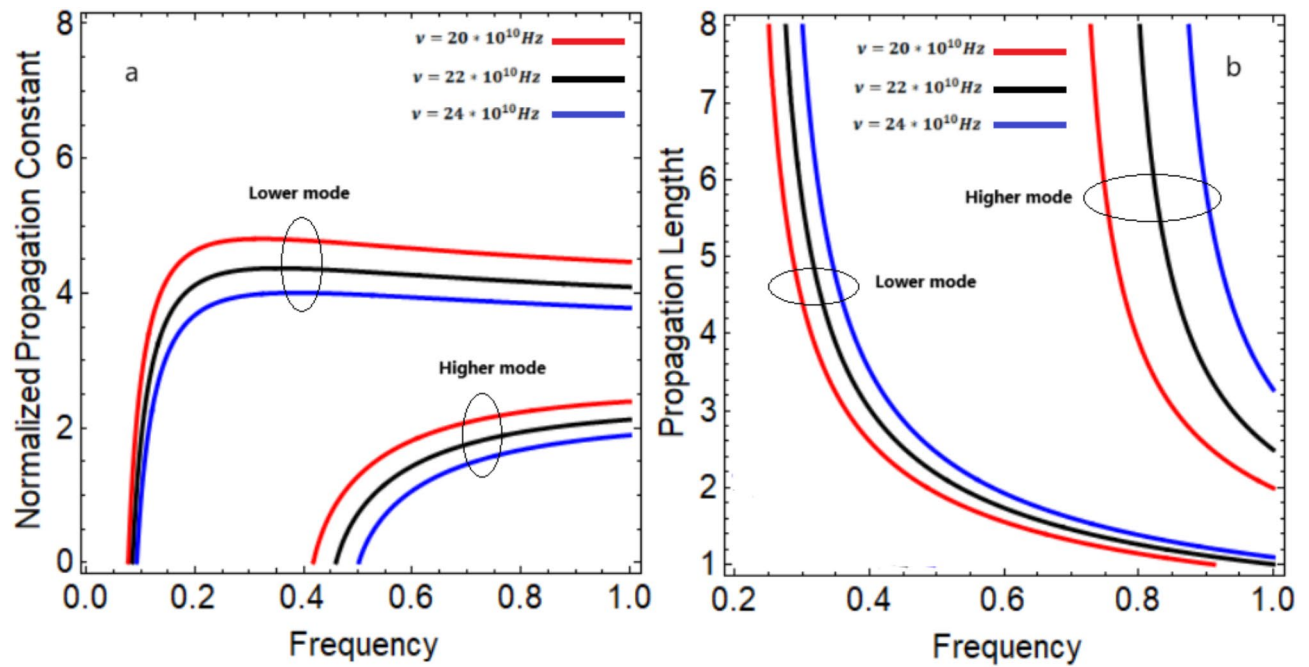
**Fig. 6**. Influence of collisional frequency on normalized propagation constant and propagation length.
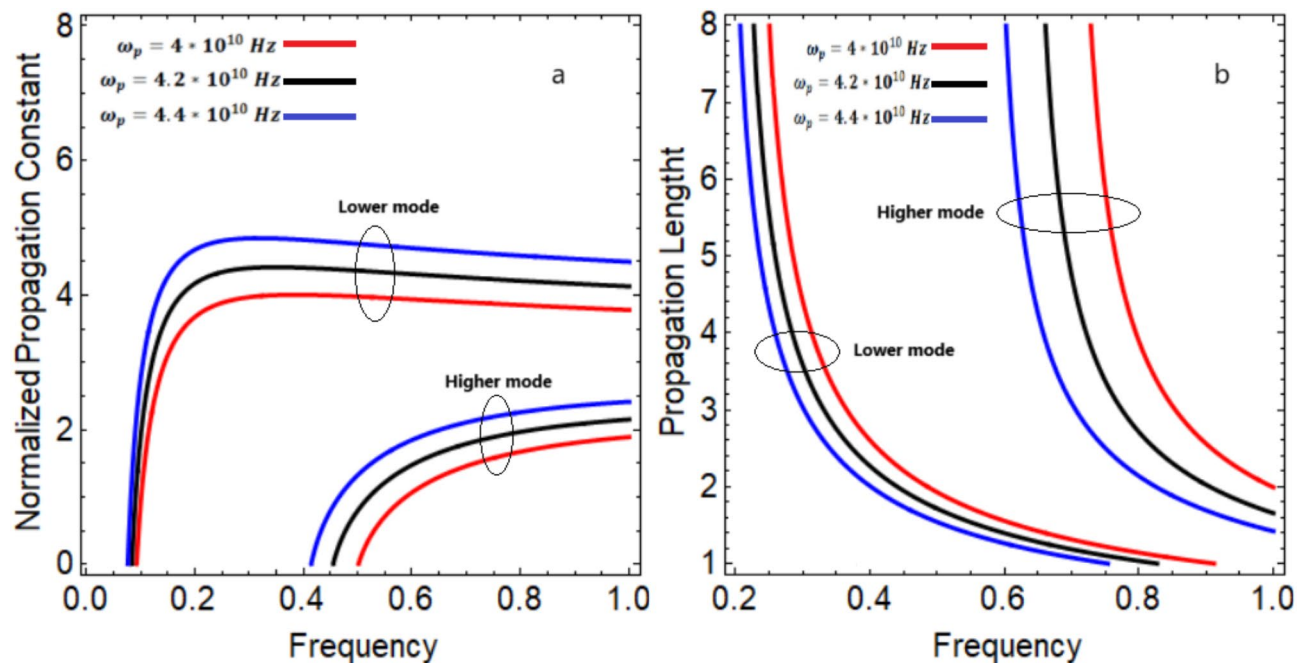


**Fig. 7**. Influence of plasma frequency on normalized propagation constant and propagation length.

a faster rate of wave propagation within the waveguide. Furthermore, higher mode exhibits higher variation in frequency band as compared to lower mode. Tailoring core width of a proposed waveguide has a profound impact on the phase velocity and field confinement of EM waves. These effects make it highly promising for sensing applications, offering opportunities for improved sensitivity, selectivity, and performance in various fields including biosensing, optical communication, and photonics. Figure 8b shows the influence of propagation length for three different values of core width. We can see that higher mode becomes more significant compared to lower mode. We also notice that lower core width values for both modes enlarge propagation length and characteristics curves shifted towards high frequency region. Figure 9a and b show the frequency dependent on normalized propagation constant and propagation length respectively. Considering Fig. 9a, higher and
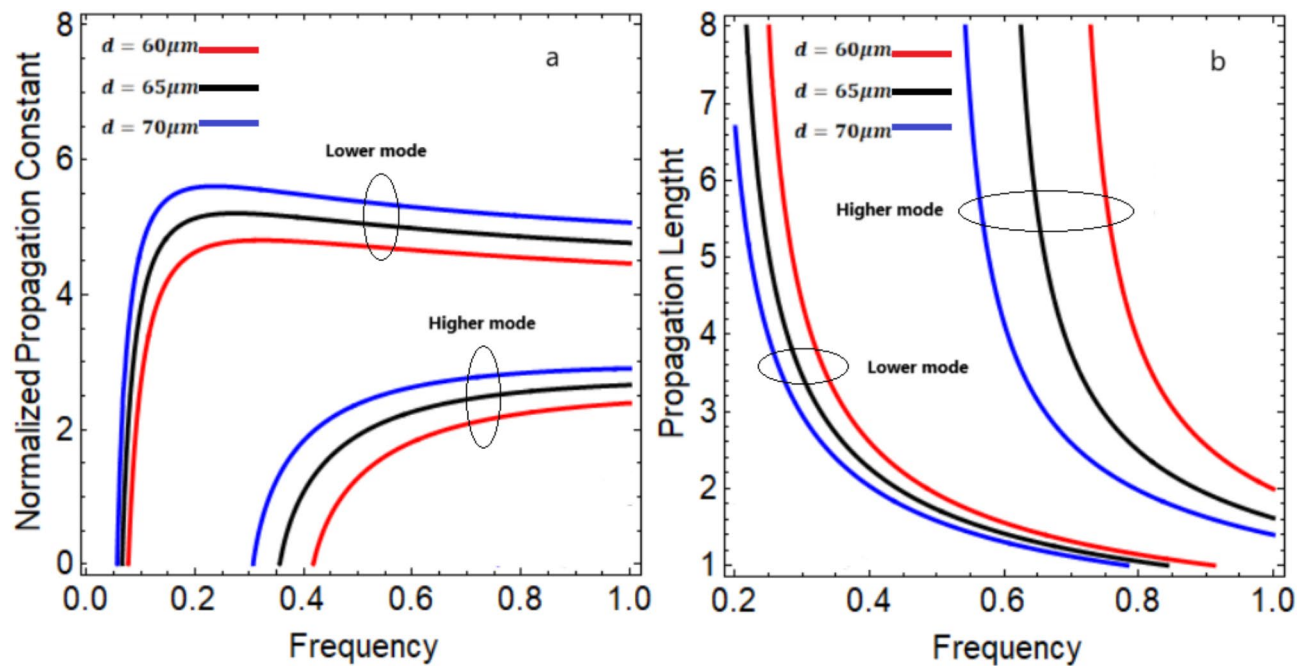
**Fig. 8**. Influence of core width on normalized propagation constant and propagation length.
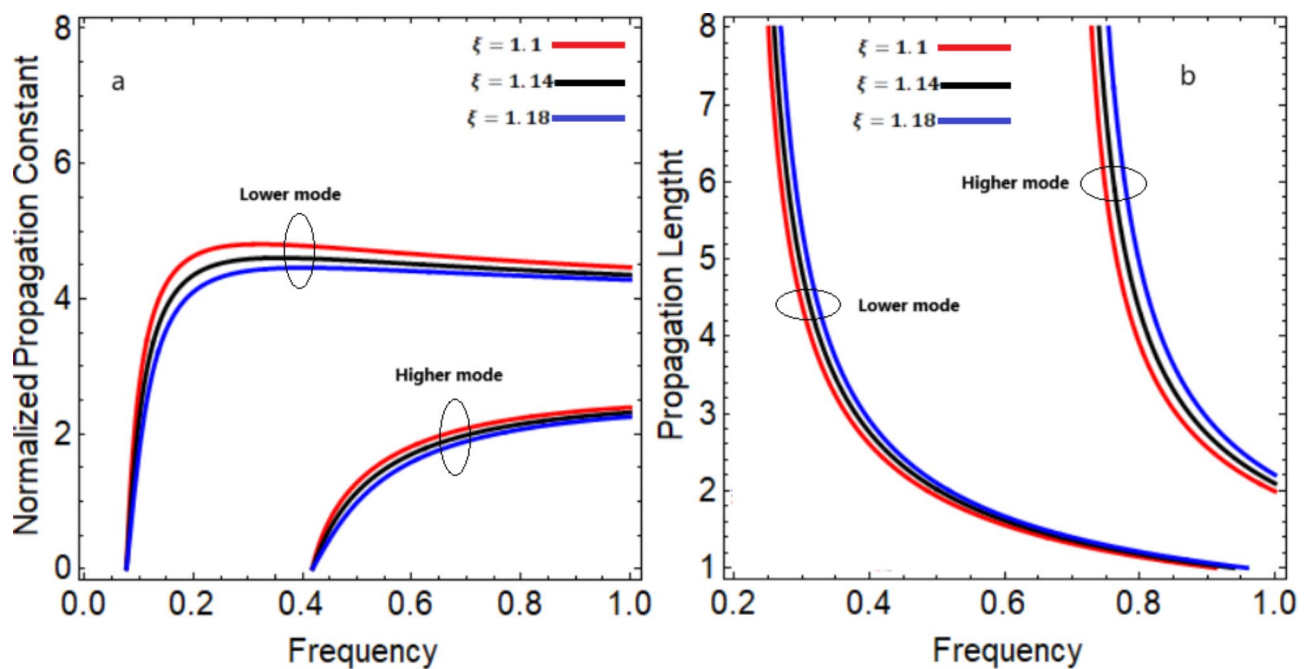


**Fig. 9**. Influence of chirality on normalized propagation constant and propagation length.

lower mode can be effectively tuned by adjusting the magnitude of chirality. As chirality increases, normalized propagation constant decreases as reported in[43]. This phenomenon has potential applications in the fabrication of chiral-based MHz devices. These devices offer unique electromagnetic properties and can be utilized in various fields, including communication, radar, and antenna technology. Figure 9b exhibits the influence of chirality on the propagation length. As chirality increases frequency band becomes narrow, and characteristics curves are shifted from low frequency to high frequency region for both modes.

## Conclusion

Electromagnetic surface wave propagated in plasma loaded uniaxial chiral waveguide and following conclusions are drawn:

1. Numerical results showed that plasma features and chirality play a crucial role in tuning the electromagnetic waves for the proposed waveguide structure.
2. Two types of uniaxial chiral media are discussed to explore EM traits of proposed waveguide structure.
3. It is concluded that normalized propagation constant and propagation length can be tuned by adjusting plasma features and uniaxial chiral parameters.
4. Case I support high frequency as compared to case II.
5. Higher normalized propagation constant could be achieved at higher values of plasma frequencies and core width for both cases. By exploiting the changes in the plasma frequency in the presence of analytes, nano-photonic sensors can achieve highly sensitive detection of chemical and biological species.
6. Higher normalized propagation constant could be achieved at lower values of collisional frequencies for both cases.
7. Higher normalized propagation constant is achieved at higher values of chirality for case I and vice versa for case II.
8. The proposed waveguide structure can be used in communication, radar, and other systems within various MHz bands.

## Data availability

Detail about data has been provided in the article.

## References

1. Jiang, C. et al. Spin–orbit-engineered selective transport of photons in plasmonic nanocircuits with panda-patterned transporters. *ACS Photon..* **9** (9), 3089–3093 (2022).
2. Nickelson, L. et al. Electrodynamical Analyses of Dielectric and Metamaterial Hollow-core CylindricalWaveguides. *Elektronika Ir. Elektrotechnika.* **82** (2), 3–8 (2008).
3. Gric, T. & Hess, O. Tunable surface waves at the interface separating different graphene-dielectric composite hyperbolic metamaterials. *Opt. Express.* **25** (10), 11466–11476 (2017).
4. Gric, T. Surface plasmons in metamaterial heterostructures. *Waves Random Complex. Media.* **31** (6), 1246–1257 (2021).
5. Yeh, C. H. et al. Cross-frequency coupling and intelligent neuromodulation. *Cyborg Bionic Syst.* **4**, 0034 (2023).
6. Yang, L. et al. Characteristics of multiple Fano resonances in waveguide-coupled surface plasmon resonance sensors based on waveguide theory. *Sci. Rep.* **8** (1), 2560 (2018).
7. Yaqoob, M. et al. Analysis of hybrid surface wave propagation supported by chiral metamaterial–graphene–metamaterial structures. *Results Phys.* **14**, 102378 (2019).
8. Zhu, C. et al. Bifurcations, chaotic behavior, and optical solutions for the complex Ginzburg–Landau equation. *Results Phys.* **59**, 107601 (2024).
9. Zhu, C. et al. On the exact soliton solutions and different wave structures to the (2 + 1) dimensional Chaffee–Infante equation. *Results Phys.* 107431 (2024).
10. Cheng, Q. & Cui, T. J. Guided modes in a planar anisotropic biaxial slab with partially negative permittivity and permeability. *Appl. Phys. Lett.* **87**(17), (2005).
11. El-Khozondar, H. J., Al-Sahhar, Z. I. & Shabat, M. M. Electromagnetic surface waves of a ferrite slab bounded by metamaterials. *AEU-Int. J. Electron. Commun.* **64** (11), 1063–1067 (2010).
12. Ghosh, S. & Pal, S. A study of plasma filled parallel plate waveguide with one boundary corrugated. *Czechoslovak J. Phys. B.* **31** (1), 25–31 (1981).
13. Liu, B. C., Yu, L. & Lu, Z. X. The surface plasmon polariton dispersion relations in a nonlinear-metal-nonlinear dielectric structure of arbitrary nonlinearity. *Chin. Phys. B.* **20** (3), 037302 (2011).
14. Prasad, R., Prasad, R. & Mantri, A. Relativistic effects on the TM-modes of one boundary corrugated parallel plate waveguide filled with uniaxial warm drifting plasma. *J. Phys.* **51** (14), 1509–1515 (1990).
15. Ghaffar, A. et al. Dispersion characteristics of surface plasmon polaritons in a graphene–plasma–graphene waveguide structure. *Can. J. Phys.* **100** (2), 123–128 (2022).
16. Qiu, Y. et al. Plasma dynamics and chlorine emission characteristics on cement pastes using collinear dual-pulse laser-induced breakdown spectroscopy. *Spectrochim. Acta Part. B: At. Spectrosc.* **209**, 106799 (2023).
17. Li, M. et al. Scaling-basis chirplet transform. *IEEE Trans. Ind. Electron.* **68** (9), 8777–8788 (2020).
18. Kui, W. et al. Design and demonstration of high-power density infrared nonlinear filtering window with EM shielding. *Opt. Express.* **32** (4), 5956–5968 (2024).
19. Zhu, C. et al. Analytical optical solutions to the nonlinear Zakharov system via logarithmic transformation. *Results Phys.* **56**, 107298 (2024).
20. Xu, G. et al. Characteristics of guided waves in indefinite-medium waveguides. *Opt. Commun.* **281** (10), 2819–2825 (2008).
21. Cao, Y. et al. Nonlinear absorption of high-power microwave pulses in a plasma filled waveguide. *Phys. Plasmas* **28**(6), (2021).
22. Zheng, L. et al. Theoretical and experimental studies of terahertz wave propagation in unmagnetized plasma. *J. Infrared Millim. Terahertz Waves.* **35**, 187–197 (2014).
23. Xu, G. & Song, Z. Interaction of terahertz waves propagation in a homogeneous, magnetized, and collisional plasma slab. *Waves Random Complex. Media.* **29** (4), 665–677 (2019).
24. Yuan, C. X. et al. FDTD analysis of terahertz wave propagation in a high-temperature unmagnetized plasma slab. *IEEE Trans. Plasma Sci.* **39** (7), 1577–1584 (2011).
25. Smirnov, Y. G. & Valovik, D. V. Guided electromagnetic waves propagating in a plane dielectric waveguide with nonlinear permittivity. *Phys. Rev. A.* **91** (1), 013840 (2015).
26. Ali, R., Zamir, B. & Shah, H. Transverse electric surface waves in a plasma medium bounded by magnetic materials. *Results Phys.* **8**, 243–248 (2018).
27. Shaikh, M., Zamir, B. & Ali, R. TE surface waves in a plasma sandwich structure. *Acta Phys. Pol. A.* **127** (6), 1625–1629 (2015).

28. Gao, N. et al. Design and performance of ultra-broadband composite meta-absorber in the 200Hz-20 kHz range. *J. Sound Vib.* **574**, 118229 (2024).
29. Cai, X. et al. Dynamically controlling terahertz wavefronts with cascaded metasurfaces. *Adv. Photon..* **3** (3), 036003 (2021).
30. Baqir, M. & Choudhury, P. Propagation through uniaxial anisotropic chiral waveguide under DB-boundary conditions. *J. Electromagn. Waves Appl.* **27** (6), 783–793 (2013).
31. Dong, J. F. & Li, J. Guided modes in the circular waveguide filled with uniaxial chiral medium. *Int. J. Appl. Electromagnet Mech.* **40** (4), 283–292 (2012).
32. Ghaffar, A. & Alkanhal, M. A. Electromagnetic reflection and transmission from a planar isotropic chiral-uniaxial chiral interface with optical axis normal to interface. *Int. J. Appl. Electromagnet Mech..* **47** (3), 805–817 (2015).
33. Ghaffar, A. et al. Radiation properties of a uniaxial chiral quadratic inhomogeneous slab under oblique incidence. *Optik* **125** (4), 1589–1597 (2014).
34. Xu, J. P. Propagation characteristics of a circular waveguide filled with a chiroferrite medium. *Int. J. Infrared Millim. Waves.* **17**, 193–203 (1996).
35. Ghaffar, A. & Alkanhal, M. A. Electromagnetic waves in parallel plate uniaxial anisotropic chiral waveguides. *Opt. Mater. Express.* **4** (9), 1756–1761 (2014).
36. Guérin, S. et al. Propagation of ultraintense laser pulses through overdense plasma layers. *Phys. Plasmas.* **3** (7), 2693–2701 (1996).
37. Rajaei, L., Mirabotalebi, S. & Shokri, B. Transmission of electromagnetic waves through a warm over-dense plasma layer with a dissipative factor. *Phys. Scr.* **84** (1), 015506 (2011).
38. Ali, M. et al. Study of hybrid surface Plasmon modes in metallic circular waveguide filled with magnetized plasma. *Waves Random Complex. Media*. **32** (1), 449–462 (2022).
39. Umair, M. et al. Transverse electric surface waves in ferrite medium surrounded by plasma layers. *J. Eur. Opt. Soc.-Rapid Publ..* **16** (1), 1–6 (2020).
40. Toqeer, I. et al. Characteristics of dispersion modes supported by Graphene Chiral Graphene waveguide. *Optik* **186**, 28–33 (2019).
41. Mi, G. & Van, V. Characteristics of surface plasmon polaritons at a chiral–metal interface. *Opt. Lett.* **39** (7), 2028–2031 (2014).
42. Shahid, M. U. et al. Propagation of electromagnetic waves in graphene-wrapped cylindrical waveguides filled with magnetized plasma. *Optik* **244**, 167566 (2021).
43. Shahid, M. U. et al. Electromagnetic waves in graphene-coated partially filled chiroplasma cylindrical waveguide. *Plasmonics*, **18**(5), 1979–1989. (2023).

## Acknowledgements

## Author contributions
Muhammad Umair wrote main manuscript and derived analytical expressions. Abdul Ghaffar and Majeed A. S. Alkanhal edited the manuscript and reviewed the numerical analysis. Yasin Khan, Muhammad Usman Shahid and Muhammad Amir Ali developed methodology in the given study. All authors reviewed the manuscript before submission.

## Funding

## Declarations

## Competing interests
The authors declare no competing interests.

## Ethical approval
Not Applicable.

## Additional information
**Correspondence** and requests for materials should be addressed to A.G.

**Reprints and permissions information** is available at www.nature.com/reprints.

**Publisher's note** Springer Nature remains neutral with regard to jurisdictional claims in published maps and institutional affiliations.